

*Analysis of a predator–prey model with
specific time scales: a geometrical approach
proving the occurrence of canard solutions*

**Jean-Christophe Poggiale, Clément
Aldebert, Benjamin Girardot & Bob
W. Kooi**

Journal of Mathematical Biology

ISSN 0303-6812

Volume 80

Combined 1-2

J. Math. Biol. (2020) 80:39-60

DOI 10.1007/s00285-019-01337-4

Your article is protected by copyright and all rights are held exclusively by Springer-Verlag GmbH Germany, part of Springer Nature. This e-offprint is for personal use only and shall not be self-archived in electronic repositories. If you wish to self-archive your article, please use the accepted manuscript version for posting on your own website. You may further deposit the accepted manuscript version in any repository, provided it is only made publicly available 12 months after official publication or later and provided acknowledgement is given to the original source of publication and a link is inserted to the published article on Springer's website. The link must be accompanied by the following text: "The final publication is available at link.springer.com".



Analysis of a predator–prey model with specific time scales: a geometrical approach proving the occurrence of canard solutions

Jean-Christophe Poggiale¹ · Clément Aldebert¹ · Benjamin Girardot¹ · Bob W. Kooi²

Received: 30 June 2018 / Revised: 21 November 2018 / Published online: 20 February 2019
© Springer-Verlag GmbH Germany, part of Springer Nature 2019

Abstract

We study a predator–prey model with different characteristic time scales for the prey and predator populations, assuming that the predator dynamics is much slower than the prey one. Geometrical Singular Perturbation theory provides the mathematical framework for analyzing the dynamical properties of the model. This model exhibits a Hopf bifurcation and we prove that when this bifurcation occurs, a canard phenomenon arises. We provide an analytic expression to get an approximation of the bifurcation parameter value for which a maximal canard solution occurs. The model is the well-known Rosenzweig–MacArthur predator–prey differential system. An invariant manifold with a stable and an unstable branches occurs and a geometrical approach is used to explicitly determine a solution at the intersection of these branches. The method used to perform this analysis is based on Blow-up techniques. The analysis of the vector field on the blown-up object at an equilibrium point where a Hopf bifurcation occurs with zero perturbation parameter representing the time scales ratio, allows to prove the result. Numerical simulations illustrate the result and allow to see the canard explosion phenomenon.

Keywords Canard solution · Blow-up · Singular perturbations · Invariant manifolds · Predator–prey dynamics

Mathematics Subject Classification 92B05 · 34C40 · 37G10 · 37N25

✉ Jean-Christophe Poggiale
jean-christophe.poggiale@univ-amu.fr

¹ MIO UM 110, Aix-Marseille Univ., Univ. Toulon, CNRS, IRD, 13288 Marseille, France

² Faculty of Science, VU Amsterdam, De Boelelaan 1085, 1081 HV Amsterdam, The Netherlands

1 Introduction

Predation allows energy to flow across ecological communities and is as such an important process in ecosystem functioning and population dynamics. This has been the attention of a huge amount of works. Consequently, predator–prey models constitute a strong basis of current ecological theories. Among these models, the Rosenzweig–MacArthur model has been widely used since the exhibition of the Enrichment Paradox (Rosenzweig 1971). This model has been analyzed and extended (see Hsu 1978 for instance). In this paper, we consider this model with two characteristic time scales associated to the prey and the predator populations. Natural systems involving several time scales are ubiquitous and taking care about time scales maybe crucial in management (Hastings 2016).

When time scales are taken into account explicitly in biological or ecological modelling, it may allow to develop methods for simplifying the mathematical analysis and understanding the dynamics of complex systems. A very common method is based on the Quasi-Steady State Approximation (QSSA) or time scale separation (Schauer and Heinrich 1983; Shoffner and Schnell 2017), which has been extensively used in enzyme kinetics or biochemical systems, with more or less success (Flach and Schnell 2006). The main principle is that if the vector of fast variables reaches an equilibrium, the corresponding variables are assumed to be almost constant and can be replaced by the equilibrium coordinates. Then only the slow variables are playing a role. From the mathematical point of view, this intuitive approach have been formalized in the singular perturbation theory (Tikhonov 1952; Hoppensteadt 1966; Fenichel 1971; Vidyasagar 1980). The interested reader can see Kuehn (2015) for a summary of methods and results in the study of slow-fast dynamics.

Geometrical Singular Perturbation theory (GSPT) has been developed on the basis of Fenichel's work (Fenichel 1971). In Jones (1994) and Wiggins (1994), general aspects of the theory are explained and illustrated with details and extensions. In Fenichel (1979), (see also Sakamoto 1992), Fenichel focuses his theorem to slow–fast dynamical systems and in Hek (2010), the interested reader can see for applications to biology. This theory provides methods to reduce the dimension of a set of differential equations involving several time scales by using invariant manifolds in the phase space. Reduction of the dynamics onto these invariant manifolds leads to decrease the dimension of the initial system to the dimension of the invariant manifolds, see Poggiale and Auger (2004) for an example where the power of GSPT is fully exploited with an accurate description of the dynamics of the complete model requiring an adapted representation of the invariant manifold. Auger et al. (2008) presents the general approach in the context of ecological modelling. Singular perturbation methods have been used to build and analyze predator–prey systems (see Poggiale and Auger 1996; Poggiale 1998; Auger et al. 2006; Poggiale et al. 2008; Cordoleani et al. 2013 for instance) and have been proved to be efficient for explaining complex dynamics in food chains (e.g. Deng 2001; Deng and Hines 2002; Kooi et al. 2002; Muratori and Rinaldi 1992; de Feo and Rinaldi 1998) or food webs (Poggiale et al. 2009).

Roughly speaking, Fenichel's theorem proves that a normally hyperbolic invariant manifold is persistent under small perturbations. It has been extended in Dumortier and Roussarie (2000) and Dumortier and Roussarie (1996) for situations where the normal

hyperbolicity is lost (see also Krupa and Szmolyan 2001b and Vidal and Francoise 2012). These papers propose a geometrical method of desingularization by blow-up of the singular points where the normal hyperbolicity is not satisfied, leading to explicitly build canard solutions. Canard phenomenon has been discovered in Benoit et al. (1981) and has been shown to occur in many systems with several time scales (e.g. Dumortier and Roussarie 1996; Krupa and Szmolyan 2001a; Vidal and Francoise 2012; Li and Zhu 2013; Pokrovskii et al. 2008; Hu et al. 2017).

In Kooi and Poggiale (2018), we showed how to find a canard solution at the turning point in Rosenzweig–MacArthur model with two time scales by using asymptotic expansion methods. This paper completes the previous one by proving that such a canard solution exists and by providing an explicit construction by means of blow-up technique. The turning point is a particular case of the general developments proposed in Dumortier and Roussarie (2000), Dumortier and Roussarie (1996) and Krupa and Szmolyan (2001b). This paper is an illustration of their method on a very common predator–prey model. Since the canard solutions occur after a Hopf bifurcation, we provide an explicit algebraic relationship between the bifurcation parameter and the small parameter representing the time scale ratio. As it can be seen in Dumortier and Roussarie (2000), citeDuRou2 and Krupa and Szmolyan (2001b), the method is general and can be used for other models. Moreover, in Rosenzweig–MacArthur model, another canard solution occurs at the point located at the intersection of the prey isocline and the vertical axis. This point corresponds to a transcritical bifurcation of the fast system and is called a transcritical singularity (see Krupa and Szmolyan 2001c for instance). It can also be dealt with a blow-up approach as we illustrate in the “Appendix” of this paper. We discuss this further in the paper.

Predator–prey models with two time scales have already been the topics of several papers and slow–fast limit cycles have already been highlighted in these models (see Rinaldi and Muratori 1992 for instance). Moreover, canard phenomena in predator–prey systems have already been mentioned or conjectured in previous works (see Ambrosio et al. 2018; Hek 2010, or Mehidi and Sari 1992 for instance) but never been analyzed in detail with a generic method. Note that in dimension 2, this is more a mathematical curiosity than an ecological feature. However, the method used here is general and can be applied to more realistic situations. In higher dimension (e.g. food chain), the method still applies and can actually explain different types of fluctuations (as mixed-mode oscillations, see for instance Brøns and Kaasen 2010 or Sadhu 2016). In this case, the canard phenomenon would help to understand food chain dynamics and then contribute to explain ecological properties.

The paper is organised as follows. In Sect. 2, the model is presented and time scales are introduced. Notations and definitions are provided in the following section and some well-known results are recalled. Section 3 states the main result and the proof follows. Phase portraits are shown for bifurcation parameter values close to where a canards explosion occurs in subsections of 3. Section 4 concludes the paper with discussions and conclusions. The “Appendix” deals with the blow-up of the transcritical singularity.

2 The model: description and generalities

2.1 Model description

Let us consider the following model (Rosenzweig–MacArthur):

$$\begin{aligned} \frac{dx}{dt} &= rx \left(1 - \frac{x}{K}\right) - \frac{ax}{b+x}y \\ \frac{dy}{dt} &= \left(e' \frac{ax}{b+x}y - m'y\right) \end{aligned}$$

and we assume that the parameters e' and m' are small, so that the dynamics of the predator is slow with respect to the prey dynamics. In order to make this explicit, we define ε a small positive dimensionless parameter and we set $e' = \varepsilon e$ and $m' = \varepsilon m'$ where e and m are rescaled conversion efficiency and mortality rate. The model reads:

$$\begin{aligned} \frac{dx}{dt} &= rx \left(1 - \frac{x}{K}\right) - \frac{ax}{b+x}y \\ \frac{dy}{dt} &= \varepsilon \left(e \frac{ax}{b+x}y - my\right) \end{aligned}$$

We shall now eliminate some parameters by nondimensionalization for simplifying the mathematical study of the model. Let $x_1 = \frac{x}{K}$, $y_1 = \frac{y}{eK}$ and $t_1 = rt$ be the new variables and $a_1 = \frac{ea}{r}$, $b_1 = \frac{b}{K}$ and $m_1 = \frac{m}{r}$ be the new parameters. We replace the variables and parameters in the previous model and we omit the index 1 in all symbols for keeping notations simple. The new model reads:

$$\begin{aligned} \frac{dx}{dt} &= x \left(1 - x - \frac{a}{b+x}y\right) \\ \frac{dy}{dt} &= \varepsilon \left(\frac{ax}{b+x} - m\right) y \end{aligned}$$

Finally, we make a last transformation in order to get a polynomial vector field. This transformation is not necessary for the method to apply, we just use it for convenience. Accordingly, since we restrict our study to the positive domain $K^+ = \{(x, y) \mid \geq 0, y \geq 0\}$, we can multiply the vector field defined by the previous differential system by the positive factor $b + x$, this does not change the trajectories in the phase space. Consequently, we now study the following system:

$$\frac{dx}{dt} = x \left(b + (1 - b)x - ay - x^2 \right) \tag{1a}$$

$$\frac{dy}{dt} = \varepsilon \left((a - m)x - mb \right) y \tag{1b}$$

We assume in this paper that $a > m$, that is the predator maximal growth rate is larger than its death rate.

2.2 General results and notations

Rosenzweig–MacArthur’s model has already been studied and the dynamics is well known. We briefly summarize some results here because they will be useful in the following section.

System (20) leaves the set K^+ invariant. In this set, the prey isoclines are the vertical axis $\{x = 0\}$ and the parabola defined by $y = \frac{(1 - x)(b + x)}{a}$. The predator isoclines are the horizontal axis $\{y = 0\}$ and the vertical straight line $\{x = \frac{mb}{a - m}\}$. Let us consider the assumption:

$$\max(b, \frac{mb}{a - m}) < 1. \tag{2}$$

Under assumption (2), the vertical predator isocline crosses the previous parabola in K^+ and there exists a positive equilibrium, which will be denoted by $E = (x_E, y_E)$ with $x_E = \frac{mb}{a - m}$ and $y_E = \frac{(1 - x_E)(b + x_E)}{a}$. Let us also denote by S_T the top of the previous parabola, its coordinates are $S_T = (x_T, y_T) = (\frac{1 - b}{2}, \frac{(1 + b)^2}{4a})$. Assumption (2) is satisfied in the entire paper.

Moreover, if the vertical predator isoclines crosses the parabola on the right of S_T then E is globally asymptotically stable in the interior of K^+ and if the intersection is on the left of S_T then E is unstable and is surrounded by a unique limit cycle in K^+ . In this case, the limit cycle attracts all trajectories starting in the interior of K^+ but E . Indeed, when the vertical predator isocline moves and crosses the top of the parabola, a Hopf bifurcation occurs.

Since we consider two time scales in this paper, the parameter ε is small and we use perturbation theory to see the shape of the trajectories when ε is very close to zero but not null. Let us start with the extreme case where $\varepsilon = 0$. Then y is a constant and the dynamics of x vanishes on the vertical axis $\{x = 0\}$ and on the parabola $\{y = \frac{1}{a}(b + x)(1 - x)\}$, which, as sets of equilibria, are invariant manifolds denoted \mathcal{M}_{10} and \mathcal{M}_{20} respectively. The intersection between the vertical axis \mathcal{M}_{10} and the parabola \mathcal{M}_{20} is the point $S_C = (x_C, y_C) = (0, \frac{b}{a})$. The maximum of the parabola \mathcal{M}_{20} is the point S_T .

At these points, the invariant sets are not normally hyperbolic: \mathcal{M}_{10} loses the normal hyperbolicity at S_C and \mathcal{M}_{20} loses the normal hyperbolicity at S_C and S_T . S_T is called a fold point because when $\varepsilon = 0$ and y increases and crosses the y -value of S_T , a fold bifurcation takes place. Geometrical Singular Perturbation Theory (GSPT), initiated by Fenichel’s work, provides mathematical results for analyzing the dynamics around invariant manifolds when they are normally hyperbolic. Extension methods have been provided for singular points on the invariant manifolds where the normal hyperbolicity is lost, which correspond to a bifurcation of the fast dynamics. Among them, the blow-up technique allows to build a new geometrical object and a new vector field on this object, by change of variables, such that for the new system, the invariant manifolds are normally hyperbolic. This is a so-called desingularization method. In this works,

we apply this approach to study the dynamics of the Rosenzweig–MacArthur model with two time scales around the singular points S_T .

The next section is devoted to the mathematical analysis of system (20) in order to show that when the Hopf bifurcation takes place, a canard solution occurs. We then describe the dynamics of the system in the phase space for small positive values of ε around the Hopf bifurcation.

3 Canard solutions in the Rosenzweig–MacArthur model with a geometrical methods

3.1 Brief description of the blow-up method, notations and definitions

In this section, we simplify the study by change of variables and explain briefly how the blow-up method works. Then we provide some notations and definitions. We start by making a new change of variables in order to move the positive equilibrium E to the origin. Note that often, when analyzing fold points like S_T , the translation is made such that the fold point is moved to the origin. Actually, here, it does not matter because as we will analyse the Hopf bifurcation at this point, S_T and E coincide at the bifurcation. Then our change of coordinates is efficient to understand the bifurcation and the occurrence of a canard phenomenon. Moreover, we denote by λ the bifurcation parameter, which is defined by $\lambda = 1 - b - 2x_E$, so that the bifurcation occurs for $\lambda = 0$. We then replace the parameter a by its expression with respect to λ , that is

$$a = m \frac{1 + b - \lambda}{1 - b - \lambda}$$

Let $X = x - x_E$ and $Y = y - y_E$ and λ defined as above, system (20) then reads:

$$\frac{dX}{dt} = (X + x_E) \left(\lambda X - m \frac{1 + b - \lambda}{1 - b - \lambda} Y - X^2 \right) \tag{3a}$$

$$\frac{dY}{dt} = \varepsilon \frac{2bm}{1 - b - \lambda} X(Y + y_E) \tag{3b}$$

We consider this system on the set $\tilde{K}^+ = \{(X, Y) | X \geq -x_E, Y \geq -y_E\}$. Note that if $b > 1$, then λ would always be negative. Thus the Hopf bifurcation can occur only when $b < 1$, we make this assumption from now. In differential system (3), there are 4 parameters. We consider λ close to 0, and $\lambda_c = 0$ is a bifurcation value for this parameter. Finally, note that x_E and y_E are combinations of parameters depending on λ , such that they are strictly positive for $\lambda = 0$.

From now, system (3) will be considered as a differential system defining a family of vector fields \mathcal{X}_μ on \tilde{K}^+ where $\mu = (\varepsilon, \lambda) \in \Lambda$ with $\Lambda = [0, \varepsilon_0] \times I$ where I is a small interval containing 0 and $\varepsilon_0 > 0$. In this family, the point $(0, 0, 0, 0) \in K^+ \times \Lambda$ is a so called **non-degenerate singular fold point**. As we previously said, Fenichel's theorem does not apply because of the loss of normal hyperbolicity. In Dumortier and Roussarie (2000) and Dumortier and Roussarie (1996), the authors develop the general approach for analyzing singular fold points in dynamical systems with two time scales. In Krupa and Szmolyan (2001b), the authors address the study of non-

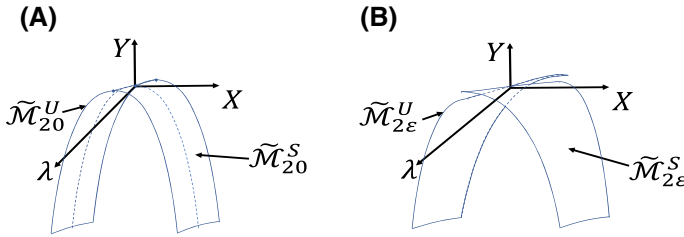


Fig. 1 Scheme of the invariant manifolds $\mathcal{M}_{2\epsilon}$ for $\epsilon = 0$ (a) and for $\epsilon > 0$ and small (b)

degenerate singular fold points and extend the previous results. Our case is thus a particular case of this general study.

To analyze this singular fold point, we complete system (3) by the equations $\frac{d\epsilon}{dt} = 0$ and $\frac{d\lambda}{dt} = 0$. We thus get a vector field in the vicinity of 0 in a 4-dimensional space, which leaves all the planes $\mathcal{P}_{u,v} = \{(X, Y, \epsilon, \lambda) | \epsilon = u, \lambda = v\}$ invariant, where u and v are any real number in a vicinity of 0.

As we already reminded, for all $\lambda \in I$, the parabola defined by $Y = \frac{(1 - b - \lambda)}{m(1 + b - \lambda)}(\lambda X - X^2)$ is invariant under the flow of \mathcal{X}_μ when $\epsilon = 0$. The union of all these parabolas constitutes an invariant 3-dimensional manifold for $\epsilon = 0$ that we denote by $\tilde{\mathcal{M}}_{20}$. We define by $\tilde{\mathcal{M}}_{20}^S$ the stable branch of the invariant manifold and $\tilde{\mathcal{M}}_{20}^U$ is the unstable branch. The former is the part of the manifold contained in the subset where $X > 0$ and $\epsilon \geq 0$ and the latter is the part of the manifold contained in the subset where $X < 0$ and $\epsilon \geq 0$, see Fig. 1. For $\epsilon = 0$, the stable branch and the unstable branch of the manifold are connected. According to Fenichel’s theorem, when the invariant manifold \mathcal{M}_{20} is normally hyperbolic, it persists for small positive values of ϵ . In other words, there exists an invariant manifold $\mathcal{M}_{2\epsilon}^S$ close to \mathcal{M}_{20}^S and an invariant manifold $\mathcal{M}_{2\epsilon}^U$ close to \mathcal{M}_{20}^U . We now have the elements to more precisely define a canard solution.

Definition 1 A solution of system (3) lying in the intersection between the stable branch and the unstable branch of $\mathcal{M}_{2\epsilon}$ is called a **maximal canard**.

Our aim in this paper is to prove that such a solution exists and the consequences on the dynamical properties of Rosenzweig–MacArthur model. In order to show that a canard phenomenon occurs in model (3), we use a blow-up approach. A blow-up is a geometrical transformation of the phase space around a singular point such that in the new geometrical object, the singular point is desingularized allowing the mathematical analysis. Note that in this paper, we focus the analysis on the canard solution arising at the top of the parabola, but in the Rosenzweig–MacArthur, another canard solution takes also place at the transcritical point located on the intersection of the parabola with the vertical axis. This set of two canard phenomenons in the same differential system is known as a canard doublet (see Pokrovskii et al. 2008). This is an important feature which leads to relaxation oscillations in the model. It may be analyzed with the blow-up approach as well (see Appendix A for some details). The canard solution arising

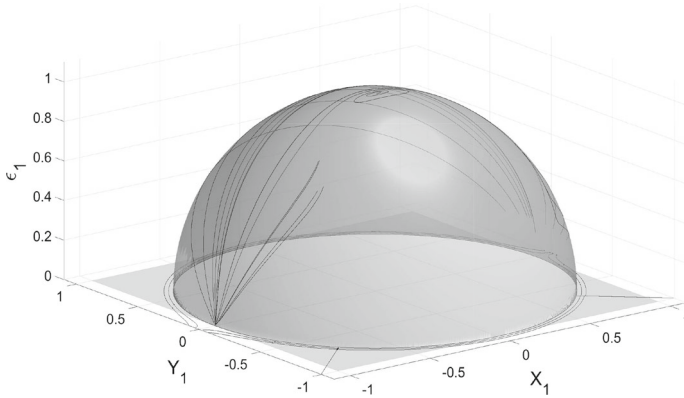


Fig. 2 Scheme of blow-up around the singularity $(0, 0, 0, 0)$ for a fixed positive λ

at the transcritical point leads to a so called delayed bifurcation (see Boudjellaba and Sari 2009; Françoise et al. 2008 or Vidal and Francoise 2012 for instance) because trajectories approaching such a point along the stable part of the vertical axis will remain a finite time along the unstable part of the vertical axis before leaving (see Muratori and Rinaldi 1992 or Vidal and Francoise 2012 for instance).

We desingularize the point $(0, 0, 0, 0) \in \tilde{K}^+ \times \Lambda$ by considering the blow-up:

$$\begin{aligned} \Psi : S^3 \times [0, +\infty[&\longrightarrow \mathbb{R}^4 \\ (X_1, Y_1, \lambda_1, \varepsilon_1, r) &\mapsto (X, Y, \varepsilon, \lambda) = (rX_1, r^2Y_1, r^2\varepsilon_1, r\lambda_1) \end{aligned}$$

where

$$X_1^2 + Y_1^2 + \lambda_1^2 + \varepsilon_1^2 = 1$$

Figure 2 illustrates the blow-up result. The singular fold point has been replaced by a hemisphere. The vector field on the horizontal set $\{\varepsilon = 0\}$ has been determined from analysis in charts $(\{X_1 = \pm 1\})$ and $(\{Y_1 = \pm 1\})$ (see details below) and then projected on the hemisphere equator (circle). This projection is done as follows. For each chart in the set $\{\varepsilon = 0\}$, we can consider that there is an axis tangent to the circle and an axis in the radial direction. We use the Poincaré compactification of the tangent axis which projects this tangent axis onto half of the circle and the radial direction is projected such that the radial distances are conserved. The vector field on the hemisphere is determined by the analysis in the chart $\{\varepsilon = 1\}$ and then projected on the sphere by Poincaré compactification.

We then start with a vector field defined on the vicinity of $0 \in \tilde{K}^+ \times \Lambda$ and we build a vector field on a geometrical object where the point 0 is replaced by a hemisphere (because $\varepsilon \geq 0$).

Firstly we write the set of ODEs after the change of coordinates where $r(t)$ is assumed to be a function of time.

$$\frac{dX_1}{dt} = \frac{1}{r} \left[\frac{dX}{dt} - X_1 \frac{dr}{dt} \right] \tag{4a}$$

$$\frac{dY_1}{dt} = \frac{1}{r^2} \left[\frac{dY}{dt} - 2rY_1 \frac{dr}{dt} \right] \tag{4b}$$

$$\frac{d\varepsilon_1}{dt} = -\frac{2\varepsilon_1}{r} \frac{dr}{dt} \tag{4c}$$

$$\frac{d\lambda_1}{dt} = -\frac{\lambda_1}{r} \frac{dr}{dt} \tag{4d}$$

where $\frac{dX}{dt}$ and $\frac{dY}{dt}$ are given in (3). In order to understand the dynamics on this hemisphere, we use charts. For instance, the chart $\{X_1 = 1\}$ describes the dynamics of the new vector field around the hemisphere (denoted by S^{3+}) for positive X_1 , the chart $\{X_1 = -1\}$ describes the dynamics around the hemisphere for negative X_1 and so on with the charts $\{Y_1 = 1\}$, $\{Y_1 = -1\}$ and $\{\varepsilon_1 = 1\}$. We first detail the chart $\{X_1 = 1\}$ for explaining the method. In the proof of theorem (1), we will just give the results for the other chart but we will provide more details for the charts $\{\varepsilon_1 = 1\}$ (for negative, null and positive λ) because it allows to understand the birth of the canard phenomenon explicitly.

To get the chart $\{X_1 = 1\}$, we consider the change of coordinates $(X, Y, \varepsilon, \lambda) = (r, r^2Y_1, r^2\varepsilon_1, r\lambda_1)$ which leads to:

$$\frac{dr}{dt} = \frac{dX}{dt} \tag{5a}$$

$$\frac{dY_1}{dt} = \frac{1}{r^2} \left[\frac{dY}{dt} - 2rY_1 \frac{dr}{dt} \right] \tag{5b}$$

$$\frac{d\varepsilon_1}{dt} = -\frac{2\varepsilon_1}{r} \frac{dr}{dt} \tag{5c}$$

$$\frac{d\lambda_1}{dt} = -\frac{\lambda_1}{r} \frac{dr}{dt} \tag{5d}$$

This is a special case of system (4) with $\frac{dX_1}{dt} = 0$ because $X_1 = 1$ hence $X = r$. After some straightforward calculations, assuming that r is small and expanding the equations with respect to r , one gets:

$$\frac{dr}{dt} = r^2 \frac{1-b}{2} \left(-1 + \lambda_1 - m \frac{1+b}{1-b} Y_1 \right) + O(r^3) \tag{6a}$$

$$\frac{dY_1}{dt} = r \left(b \frac{1+b}{2} \varepsilon_1 - Y_1(1-b)(\lambda_1 - 1 - m \frac{1+b}{1-b} Y_1) \right) + O(r^2) \tag{6b}$$

Let us consider the case $\varepsilon_1 = 0$ and $\lambda_1 = 0$ in the previous system, and after division by r , one gets:

$$\frac{dr}{dt} = r \frac{1-b}{2} \left(-1 - m \frac{1+b}{1-b} Y_1 \right) + O(r^2) \tag{7a}$$

$$\frac{dY_1}{dt} = -Y_1(1-b) \left(-1 - m \frac{1+b}{1-b} Y_1 \right) + O(r) \tag{7b}$$

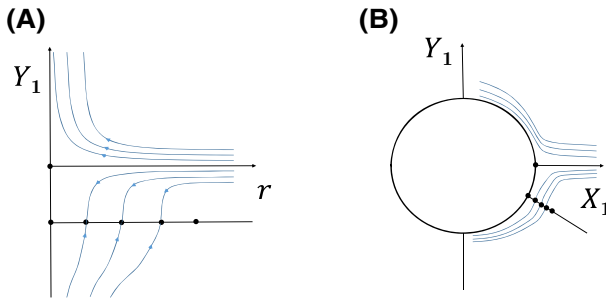


Fig. 3 Scheme of the dynamics in a chart $\{X_1 = 1\}$ for $\varepsilon_1 = 0$ and $\lambda_1 = 0$, given by system (7) (a). **b** Illustrates the transformation of the dynamics around the hemisphere in the plane $\varepsilon_1 = 0$ and $\lambda_1 = 0$, provided by the study in the previous chart $\{X_1 = 1\}$. Black points correspond to equilibria

Note that dividing by r for $r > 0$ does not change the trajectories and allows to determine the dynamics around the hemisphere and this is why we can desingularize the origin. The study of the dynamics is simple and the main results are that the vertical axis is invariant as well as the straight line defined by $Y_1 = -\frac{1-b}{m(1+b)}$. These invariant sets in the chart $\{X_1 = 1\}$ correspond to invariant sets on the blown-up geometrical object, namely respectively to the hemisphere equator (circle) and to the stable branch of the parabola (straight lines perpendicular to the circle), in the plane $\{\varepsilon_1 = 0\} \cap \{\lambda_1 = 0\}$. Results are illustrated in Fig. 3.

3.2 Main results

Theorem 1 For $\varepsilon > 0$ small enough, system (20) admits maximal canard solutions when λ becomes positive and close to zero. More precisely, there exists a function defined in the vicinity of $0 \in \mathbb{R}$ with $\varepsilon \mapsto \lambda_{1c}(\varepsilon)$ such that for all $\varepsilon > 0$ close to 0, there exists $\lambda = \lambda_c(\varepsilon) > 0$ for which system (20) exhibits a maximal canard. An approximation of this function is provided by:

$$\lambda_c(\varepsilon) = \frac{mb(1+b)^2}{(1-b)^3} \varepsilon + O(\varepsilon^{3/2})$$

Proof The proof mainly rests on the blow-up of the fold point. We first complete the blow-up with all the needed charts and focus on the study in chart $\{\varepsilon = 1\}$ for different values of λ around 0.

In chart $\{X_1 = -1\}$, and after division by r , the vector field around the hemisphere is provided by:

$$\frac{dr}{dt} = r \frac{1-b}{2} \left(\lambda_1 + 1 + m \frac{1+b}{1-b} Y_1 \right) + O(r^2) \tag{8a}$$

$$\frac{dY_1}{dt} = -\varepsilon_1 b \frac{1+b}{2} - Y_1 r (1-b) (1 + \lambda_1 + Y_1 m \frac{1+b}{1-b}) + O(r) \tag{8b}$$

$$\frac{d\varepsilon_1}{dt} = \varepsilon_1(1 - b)(1 + \lambda_1 + mY_1 \frac{1 + b}{1 - b}) + O(r) \tag{8c}$$

$$\frac{d\lambda_1}{dt} = -\lambda_1 \frac{1 - b}{2} (1 + \lambda_1 + m \frac{1 + b}{1 - b}) + O(r) \tag{8d}$$

Note that in the plane $\varepsilon_1 = 0$ and $\lambda_1 = 0$, this system leaves the straight line defined by $Y_1 = -\frac{1-b}{m(1+b)}$ invariant. This straight line corresponds to the unstable branch of the parabola in the initial blow-up geometrical object.

In chart $\{Y_1 = 1\}$, and after division by r , the vector field around the hemisphere is provided by:

$$\frac{dX_1}{dt} = \frac{1 - b}{2} (\lambda_1 X_1 - m \frac{1 + b}{1 - b} - X_1^2) - \varepsilon_1 \frac{(1 + b)b}{4} X_1^2 + O(r) \tag{9a}$$

$$\frac{dr}{dt} = r\varepsilon_1 \frac{(1 + b)b}{4} X_1 + O(r^2) \tag{9b}$$

$$\frac{d\varepsilon_1}{dt} = -2\varepsilon_1^2 \frac{(1 + b)b}{4} X_1 + O(r) \tag{9c}$$

$$\frac{d\lambda_1}{dt} = -\lambda_1 \varepsilon_1 \frac{(1 + b)b}{4} X_1 + O(r) \tag{9d}$$

In chart $\{Y_1 = -1\}$, and after division by r , the vector field around the hemisphere is provided by:

$$\frac{dX_1}{dt} = \frac{1 - b}{2} (\lambda_1 X_1 + m \frac{1 + b}{1 - b} - X_1^2) + \varepsilon_1 \frac{(1 + b)b}{4} X_1^2 + O(r) \tag{10a}$$

$$\frac{dr}{dt} = -r\varepsilon_1 \frac{(1 + b)b}{4} X_1 + O(r^2) \tag{10b}$$

$$\frac{d\varepsilon_1}{dt} = -2\varepsilon_1^2 \frac{(1 + b)b}{4} X_1 + O(r) \tag{10c}$$

$$\frac{d\lambda_1}{dt} = -\lambda_1 \varepsilon_1 \frac{(1 + b)b}{4} X_1 + O(r) \tag{10d}$$

Note that in the plane $\varepsilon_1 = 0$ and $\lambda_1 = 0$, this system leaves the straight lines defined by $X_1 = \pm\sqrt{\frac{m(1+b)}{1-b}}$ invariant. These straight lines correspond to the stable and unstable branches of the parabola. Indeed, it can be noticed that on these lines, $X_1^2 = \frac{m(1+b)}{1-b}$ which is the negative reciprocal of Y_1 on the invariant straight lines in charts $\{X_1 = \pm 1\}$.

Putting all the charts together and mapping the results onto the blown up object allows to understand the dynamics around the hemisphere. This is actually equivalent to the dynamics of the initial system (3) around the origin. The result is illustrated on Fig. 4.

We now need to analyze the dynamics for positive and small ε . This is done by using the charts $\{\varepsilon_1 = 1\}$ with different values of λ_1 around 0. In chart $\{\varepsilon_1 = 1\}$, and after division by r , the vector field around the hemisphere is provided by:

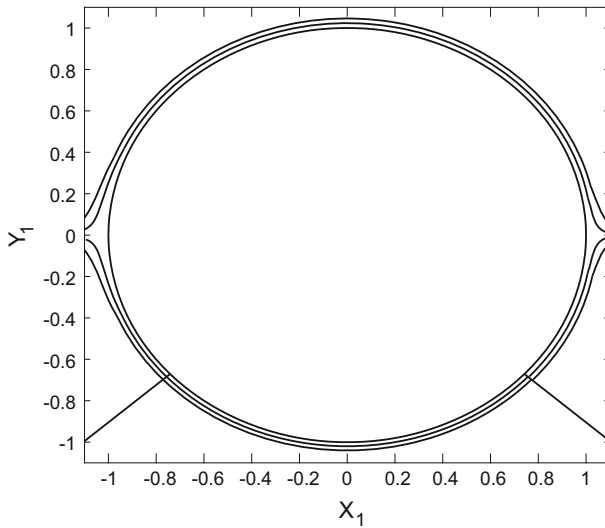


Fig. 4 Simulation of the vector field on the blown-up object in the phase plane $\varepsilon = 0$ and $\lambda_1 = 0$. Simulations have been made in each chart and then the trajectories have been mapped onto the blown up object. The full circle is the equator of the hemisphere

$$\frac{dX_1}{dt} = \frac{1-b}{2}(\lambda_1 X_1 - m \frac{1+b}{1-b} Y_1 - X_1^2) + O(r) \tag{11a}$$

$$\frac{dY_1}{dt} = \frac{(1+b)b}{2} X_1 + O(r) \tag{11b}$$

The dynamics on the hemisphere is obtained by setting $r = 0$ in the previous system. Let us start with $\lambda_1 = 0$. The origin $(X_1, Y_1) = (0, 0)$ is the only equilibrium and the vector field is symmetric with respect to the vertical axis of coordinates $X_1 = 0$. The origin is a centre, as we will see by exhibiting a Lyapunov function. Moreover, the parabola \mathcal{P} defined by $Y_1 = -\frac{1-b}{m(1+b)} X_1^2 + \frac{b(1+b)}{2(1-b)}$ is invariant under the flow. And when $X_1 \sim \pm\infty$, the parabola equation is equivalent to $Y_1 = -\frac{1-b}{m(1+b)} X_1^2$ and indeed it collapses at infinity on the straight lines found in the previous charts associated to this parabola. The dynamics is illustrated on Fig. 5.

We define the Hamiltonian function H as follows:

$$H(X_1, Y_1) = \exp\left(\frac{2(1-b)}{b(1+b)} Y_1\right) \left(X_1^2 + \frac{m(1+b)}{1-b} Y_1 - \frac{mb(1+b)^2}{2(1-b)^2}\right) \tag{12}$$

This function vanishes on the parabola \mathcal{P} and is positive below the parabola. The level curves of H correspond to trajectories of system (11) when $\lambda_1 = 0$. Let denote by γ the trajectory on the hemisphere, it connects the stable branch \mathcal{M}_{20}^S to the unstable branch \mathcal{M}_{20}^U on the equator of the hemisphere. Along this trajectory, H remains equal to 0. Let us parameterize γ as a function of time.

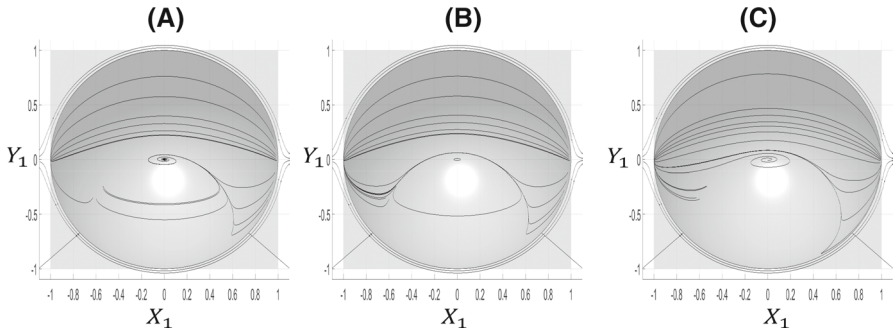


Fig. 5 Illustration of the dynamics induced by the vector field on the blown up object for three values of λ_1 in the chart $\{\varepsilon_1 = 1\}$. In **a**, $\lambda_1 < 0$, 0 is a stable equilibrium attracting trajectories initiated under the parabola \mathcal{P} , while trajectories initiated above this parabola leave the hemisphere by the West point. In **b**, $\lambda_1 = 0$, the origin is a centre. All trajectories initiated below the parabola \mathcal{P} are closed curves surrounding the origin. The trajectories initiated above the parabola leave the hemisphere by the West point. The parabola is invariant under the flow. In **c**, $\lambda_1 > 0$ and the origin is an unstable focus. All trajectories leave the hemisphere by the West point. The parameter values used for these simulations are $b = 0.1$, $m = 1$ and $\lambda_1 = -0.1$ in **(a)**, $\lambda_1 = 0$ in **(b)** and $\lambda_1 = 0.1$ in **(c)**

Lemma 1 *The curve γ can be parameterized as follows:*

$$\gamma(t) = \left(-\frac{1-b}{m(1+b)}t^2 + \frac{b(1+b)}{2(1-b)} \right)$$

The proof of the lemma is straightforward since all $(X_1(t), Y_1(t))$ belonging to γ satisfy the equation of \mathcal{P} , thus $H(\gamma(t)) = 0$. The theorem claims that for all small $\varepsilon > 0$, there exists a value of λ such that the unstable manifold and stable manifold are connected. Actually, the connection will be established from γ . We first denote by $\tilde{\mathcal{M}}_{2\varepsilon}^S$ (resp. $\tilde{\mathcal{M}}_{2\varepsilon}^U$) the stable (resp. unstable) branch of the invariant manifold in the chart $\{\varepsilon_1 = 1\}$. We will then prove that for all sufficiently small ε , there exists a value of λ for which the distance between these manifolds vanishes. We need other notations for expressing this distance, which will follow from the expansion of the differential system (11) in chart $\{\varepsilon_1 = 1\}$ to order 1 in r . One gets:

$$\begin{aligned} \frac{dX_1}{dt} &= \frac{1-b}{2}(-m\frac{1+b}{1-b}Y_1 - X_1^2) + \frac{1-b}{2}\lambda_1 X_1 - r\left(X_1^3 + \frac{m(1+b)}{1-b}X_1 Y_1\right) + O(r(\lambda_1 + r)) \\ \frac{dY_1}{dt} &= \frac{(1+b)b}{2}X_1 + O(r(\lambda_1 + r)) \end{aligned}$$

The right hand-side of this system will be denoted as follows:

$$F(X_1, Y_1, r, \lambda_1) = F_0(X_1, Y_1) + rF_{1,r}(X_1, Y_1) + \lambda_1 F_{1,\lambda_1}(X_1, Y_1) + O(r(\lambda_1 + r)) \tag{13}$$

with

$$F_0(X_1, Y_1) = F(X_1, Y_1, 0, 0)$$

$$\begin{aligned}
 F_{1,r}(X_1, Y_1) &= \frac{\partial F}{\partial r}(X_1, Y_1, 0, 0) \\
 F_{1,\lambda_1}(X_1, Y_1) &= \frac{\partial F}{\partial \lambda_1}(X_1, Y_1, 0, 0)
 \end{aligned}$$

In order to calculate the distance between the stable and unstable branch of the invariant manifold in the chart $\{\varepsilon_1 = 1\}$, we calculate the deviation of the value taken by $H(t)$ along the whole curve γ for every $(r, \lambda_1) \simeq (0, 0)$. The distance between $\mathcal{M}_{2\varepsilon}^S$ and $\mathcal{M}_{2\varepsilon}^U$ is:

$$\delta(r, \lambda_1) = \int_{H(\gamma(-\infty))}^{H(\gamma(+\infty))} dH(\gamma(t)) = \int_{-\infty}^{+\infty} \frac{dH(\gamma(t))}{dt} dt \tag{14}$$

Now, we can write $\frac{dH}{dt} = \nabla H \cdot F = \nabla H \cdot (F_0 + rF_{1,r} + \lambda_1 F_{1,\lambda_1} + O(r(\lambda_1 + r)))$ and since H is a first integral of the vector field with $r = 0$ and $\lambda_1 = 0$, then $\nabla H \cdot F_0 = 0$. It follows:

$$\delta(r, \lambda_1) = \alpha_r r + \alpha_{\lambda_1} \lambda_1 + O(r(r + \lambda_1)) \tag{15}$$

where $\alpha_r = \int_{-\infty}^{+\infty} \nabla H(\gamma(t)) \cdot F_{1,r}(\gamma(t)) dt$ and $\alpha_{\lambda_1} = \int_{-\infty}^{+\infty} \nabla H(\gamma(t)) \cdot F_{1,\lambda_1}(\gamma(t)) dt$.

Lemma 2 *There exists a function λ_{1c} depending on r in a neighborhood of 0 such that $\delta(r, \lambda_{1c}(r)) = 0$.*

This lemma proves the existence of canard solutions. Its own proof is based on the implicit function theorem. Since $\delta(0, 0) = 0$, we just need to show that $\frac{d\delta}{d\lambda_1}(0, 0) \neq 0$, or with the above notations that $\alpha_{\lambda_1} \neq 0$.

Using the previous expression for α_{λ_1} and replacing $\gamma(t)$ by its time parametrization, one gets:

$$\alpha_{\lambda_1} = e(1 - b) \int_{-\infty}^{+\infty} \exp(-At^2) t^2 dt \tag{16}$$

where $A = \frac{2(1 - b)^2}{mb(1 + b)^2}$ and after integration by parts, we obtain $\alpha_{\lambda_1} = \frac{e(1 - b)}{2A} \sqrt{\frac{\pi}{A}} \neq 0$, thus the Implicit Functions theorem applies and Lemma (2) is proved.

In order to complete the Proof of Theorem (1), we use Eq. (17) where the distance vanishes, thus:

$$\lambda_{1c}(r) = -\frac{\alpha_r}{\alpha_{\lambda_1}} r + O(r^2) \tag{17}$$

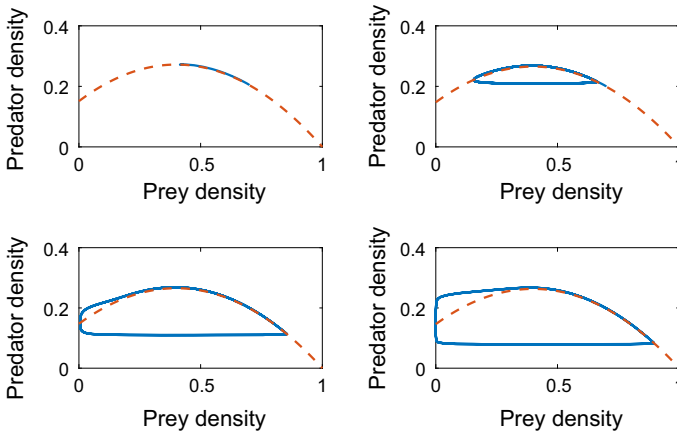


Fig. 6 Several phase portraits showing the birth of the limit cycle in the Hopf bifurcation with a canard phenomenon. On the top left panel, an equilibrium point close to the top of the parabola is globally asymptotically stable. On the top right panel, just after the Hopf bifurcation, a small limit cycle is present. On the bottom left panel, the limit cycle amplitude is drastically enlarged (canard explosion) while the bifurcation parameter is still very close to the value used on the top right panel. Note that the trajectory remains along the unstable branch of the parabola during a finite time. On the bottom right panel, the limit cycle is the largest one. The parameter values used for these simulations are $b = 0.2$, $m = 0.9$ and $\lambda = -0.05$ in top-left, $\lambda = 0.0112$ in top-right, $\lambda = 0.01123$ in bottom-left and $\lambda_1 = 0.03$ in bottom-right. For each panel, $\varepsilon = 0.02$

For calculating α_r , we proceed as for α_{λ_1} and one gets $\alpha_r = -\frac{e}{A^2} \sqrt{\frac{\pi}{A}}$ where A is defined as previously, thus:

$$\lambda_{1c}(r) = \frac{mb(1+b)^2}{(1-b)^3} r + O(r^2) \tag{18}$$

Finally, since $r = \sqrt{\varepsilon}$ and $\lambda = \sqrt{\varepsilon} \lambda_1$, we conclude:

$$\lambda_c(\sqrt{\varepsilon}) = \frac{mb(1+b)^2}{(1-b)^3} \varepsilon + O(\varepsilon^{3/2}) \tag{19}$$

This proves Theorem (1).

3.3 Numerical simulations

In Fig. 6 the phase portraits are shown for various values of the bifurcation parameter λ and a fixed $\varepsilon = 0.02$ value. These numerical simulations illustrate the canard explosion phenomenon where for the intermediate parameter values the small limit cycle disappears suddenly (between $\lambda = 0.0112$ and $\lambda = 0.01123$) and is replaced by a big limit cycle. Similar plots with smaller ε -values indicate that the canard explosion occurs for smaller, but positive, λ values and furthermore that the transition becomes also sharper. That is, the shape of the limit cycles in the phase-space is closer to that

of the relaxation oscillations. These characteristic cycles consist of two fast horizontal episodes and two slow episodes, one downwards along the vertical axis and one upwards along the branch of the parabola.

3.4 Comparison of formula (19) with formula (47) in Kooi and Poggiale (2018)

We now compare our result in formula (19) with the result we obtained with a different approach in formula (47) in Kooi and Poggiale (2018). In that paper, Rosenzweig–MacArthur model with two time scales is also analyzed by using asymptotic expansions of the invariant manifolds. Since the functional response of the predator–prey model is not exactly of the same form, we remind here the algebraic relationship between the parameters of the model in Kooi and Poggiale (2018), namely a_1, b_1, d and ε and the parameters of the present paper, namely a, b, m and ε , the relation is $(a_1, b_1, d, \varepsilon) = (a/b, 1/b, m, \varepsilon)$.

Since we define here λ by $\lambda = 1 - b - 2x_E$, by replacing a and b by their expression with respect to a_1 and b_1 and considering that in Kooi and Poggiale (2018) the assumptions $a_1 = \frac{5}{3}b_1$ and $d = 1$ have been made, one gets that $b_1 = \frac{4}{1 - \lambda}$ and since $\lambda \simeq 0$ then $b_1 = 4 + 4\lambda + O(\lambda^2)$.

If we replace λ by λ_c (formula 19) we obtain $b_1 = 4 + 4\frac{(1 + b_1)^2}{(b_1 - 1)^3}\varepsilon + \dots$ and taking $b_1 = 4 + O(\varepsilon)$ as in Kooi and Poggiale (2018), this gives:

$$b_1 = 4 + \frac{100}{27}\varepsilon + \dots$$

This is exactly the first order term found in formula (47) in Kooi and Poggiale (2018). Observe that here the expansion is in $\sqrt{\varepsilon}$ while in Kooi and Poggiale (2018) it was in ε . Because the $\sqrt{\varepsilon}$ -term is missing and the first term is the $(\sqrt{\varepsilon})^2 = \varepsilon$ -term in (19) makes this comparison possible. Note that in Krupa and Szmolyan (2001b) it is mentioned that the expansion is a power series in ε and that is related to a time reversal symmetry property of the blow-up transformation.

4 Discussion and conclusion

In this paper, the Rosenzweig–MacArthur model with two time scales has been studied to show that a maximal canard solution exists for small ε . The proof is based on a blow-up method which could allow us to build the canard solution explicitly. A relation between the Hopf bifurcation parameter λ and the small parameter ε has been determined and it permits to get an approximation of λ for which the canard solutions arise.

Once our results have been demonstrated, we proposed a comparison with what has been obtained in our previous work Kooi and Poggiale (2018), showing that both methods provide similar results at the first order in the asymptotic expansion with respect to ε . Since the relation obtained here is a function of $\sqrt{\varepsilon}$ while the relation

obtained in our previous work is a function of ε , we can't easily push the comparison further.

Note that the range of values for λ in Fig. 6 is very small. Moreover, between panel top-right ($\lambda = 0.0112$) and panel bottom-left ($\lambda = 0.01123$) the change in λ value is very small. This corresponds to a canard explosion, the shape of the canard solution forming the limit cycle in the first case is very different that the shape in the second case, the amplitude of the limit cycle drastically increased between these simulations. This is a very well known phenomenon and this is why finding such canard solution is not obvious if we do not know for which parameter value it occurs. Relations like formula (19) in our paper, or like formula (47) in Kooi and Poggiale (2018) are therefore useful.

The bifurcation pattern of the Rosenzweig–MacArthur model is simple. For interior steady states either a globally stable equilibrium or limit cycle takes place. For $\varepsilon > 0$ the Hopf-theorem applies and shows how the limit cycle emanates at the Hopf bifurcation point where $\lambda = 0$ which occurs at the top S_T of the prey isocline being a parabola in the phase space. For $\lambda < 0$ we have an equilibrium because the Quasi-Steady State Assumption (QSSA) approach is valid where this equilibrium point is closely approached along the stable branch of the parabola.

On the other hand, when $\lambda > 0$ the equilibrium is on the unstable branch. Then in the limiting case where $\varepsilon \ll 1$ the shape of the emerging limit cycle is, however, not the well-know cycle but it is distorted by the difference in time scales for the dynamics in the fast prey (horizontal) and slow predator (vertical) direction leading to a relaxation oscillation. Therefore the classical Hopf bifurcation analysis has to be replaced by a blow-up analysis as performed in this paper. In this analysis the top S_T of the parabola acts as a fold bifurcation. The blow-up technique reveals that the limit cycles follows the initially unstable branch of the parabola which in the blow-up setting is stable in a restricted range for the top S_T . The shape of the limit cycle looks like a top part of the parabola at the top and a horizontal line at the bottom. For small ε -values these effects occur and remain visible also for larger values of ε as well as bifurcation increasing λ -values until it give rise to the canard explosion (see Fig. 6) where the small limit cycle disappears abruptly within a small λ parameter range.

In Krupa and Szmolyan (2001b) also the blow-up technique is used to study the canard phenomenon. Like the approach in this paper they follow the work on blow-up theory in Dumortier and Roussarie (2000) and Dumortier and Roussarie (1996). Our approach is similar to that used in those references.

Interestingly, the method is general and can be applied to other models. For instance, in Ambrosio et al. (2018) the modified Leslie–Gower predator–prey model where the prey reproduces much faster than the predator, is studied. It is stated that for the slow-fast system, the dynamics near the top of the predator parabola isocline needs not to be analyzed with respect to canard explosions. However, numerical simulations (not shown here) show that there is a canard explosion very similar to that observed here for the Rosenzweig–MacArthur predator–prey model shown in Fig. 6. Blow-up methods could extend the results provided in Ambrosio et al. (2018).

Acknowledgements The authors acknowledge two anonymous referees and Odo Diekmann for the constructive comments and suggestions which helped us to improve the manuscript.

5. Appendix

In this ‘‘Appendix’’, we prove that a canard solution exists in the vicinity of the point S_C located at the intersection of the parabola and the vertical axis in the Rosenzweig–MacArthur model. Let us start with system (1):

$$\frac{dx}{dt} = x \left(b + (1 - b)x - ay - x^2 \right) \tag{20a}$$

$$\frac{dy}{dt} = \varepsilon \left((a - m)x - mb \right) y \tag{20b}$$

The point S_C corresponds to a point where the fast dynamics exhibits a transcritical bifurcation when the slow variable y decreases: for $y > \frac{b}{a}$, $x = 0$ is stable for the fast equation while for $y < \frac{b}{a}$, $x = 0$ is unstable for the fast equation. In other words, S_C is at the intersection of the invariant manifolds \mathcal{M}_{10} (the y -axis) and \mathcal{M}_{20} (the parabola). As in the article, by adding $\frac{d\varepsilon}{dt} = 0$ to system (20), we get a 3-dimensional system. By Fenichel’s theorem, \mathcal{M}_{10} and \mathcal{M}_{20} persist for small positive ε at each point where they are normally hyperbolic. It is not the case in S_C . In Boudjellaba and Sari (2009), Franoise et al. (2008), Krupa and Szmolyan (2001c) and Vidal and Franoise (2012) for instance, the authors address the problem of this type of singularity. Our case is not considered in Krupa and Szmolyan (2001c).

Again, the blow-up replaces the point S_C by a geometrical object (a hemisphere here) on which all points are non singular (the normal hyperbolicity is reached). Even if it is quite obvious in this example, one will see that the stable branch of \mathcal{M}_{10} is connected to the unstable branch of \mathcal{M}_{10} by a trajectory of the blown-up vector field, this is actually due to the fact that the vertical axis is invariant for the complete system (20). This connection leads to a canard solution. In this case, the canard solution gives birth to a so-called delayed bifurcation (see Franoise et al. 2008; Boudjellaba and Sari 2009 and Vidal and Franoise 2012), those works do not use blow-up method for their analysis.

We translate the point S_C at the origin with the following change of coordinates $(X, Y) = (x, y - b/a)$, the new system reads:

$$\frac{dX}{dt} = X \left((1 - b)X - aY - X^2 \right) \tag{21a}$$

$$\frac{dY}{dt} = \varepsilon \left(Y + \frac{b}{a} \right) \left((a - m)X - mb \right) \tag{21b}$$

In order to study the singularity, where the normal hyperbolicity is lost, we use the following blow-up:

$$(X, Y, \varepsilon) = (rX_1, rY_1, r^2\varepsilon_1)$$

where $X_1^2 + Y_1^2 + \varepsilon_1^2 = 1$ and $r \in [0, r_0)$ with $r_0 > 0$. As explained in the article, we study the dynamics by using charts.

In chart $\{X_1 = 1\}$, we have: $X = r, Y = rY_1$ and $\varepsilon = r^2\varepsilon_1$, and after division by r for desingularization, the system reads:

$$\frac{dr}{dt} = r(1 - b - aY_1) + O(r^2) \tag{22a}$$

$$\frac{dY_1}{dt} = \varepsilon_1 \frac{b^2m}{a} - Y_1(1 - b - aY_1) + O(r) \tag{22b}$$

$$\frac{d\varepsilon_1}{dt} = -2\varepsilon_1(1 - b - aY_1) + O(r) \tag{22c}$$

In chart $\{Y_1 = 1\}$, we have : $X = rX_1, Y = r$ and $\varepsilon = r^2\varepsilon_1$, and after division by r for desingularization, the system reads:

$$\frac{dr}{dt} = -r\varepsilon_1 \frac{mb^2}{a} + O(r^2) \tag{23a}$$

$$\frac{dX_1}{dt} = X_1((1 - b)X_1 - a + \varepsilon_1 \frac{mb^2}{a}) + O(r) \tag{23b}$$

$$\frac{d\varepsilon_1}{dt} = 2\varepsilon_1^2 \frac{mb^2}{a} + O(r) \tag{23c}$$

In chart $\{Y_1 = -1\}$, we have : $X = rX_1, Y = -r$ and $\varepsilon = r^2\varepsilon_1$, and after division by r for desingularization, the system reads:

$$\frac{dr}{dt} = r\varepsilon_1 \frac{mb^2}{a} + O(r^2) \tag{24a}$$

$$\frac{dX_1}{dt} = X_1((1 - b)X_1 + a - \varepsilon_1 \frac{mb^2}{a}) + O(r) \tag{24b}$$

$$\frac{d\varepsilon_1}{dt} = -2\varepsilon_1^2 \frac{mb^2}{a} + O(r) \tag{24c}$$

In chart $\{\varepsilon_1 = 1\}$, we have : $X = rX_1, Y = rY_1$ and $\varepsilon = r^2$, and after division by r for desingularization, the system reads:

$$\frac{dX_1}{dt} = X_1((1 - b)X_1 - aY_1) + O(r) \tag{25a}$$

$$\frac{dY_1}{dt} = -\frac{mb^2}{a} + O(r) \tag{25b}$$

Note that since we are not interested in the dynamics of the system for negative values of X , we don't use the chart $\{X_1 = -1\}$ and focus on the hemisphere contained in $X_1 > 0$.

Figure 7 illustrates the result of the blow-up. The disk in the center represents the hemisphere $\{(X_1, Y_1, \varepsilon_1), X_1^2 + Y_1^2 + \varepsilon_1^2 = 1, \varepsilon_1 \geq 0\}$. The circle of radius one is the equator of this hemisphere. The remaining part of the diagram corresponds to the plane $\{\varepsilon = 0\}$ minus the origin (the point S_C). In this plane, the dynamics is equivalent

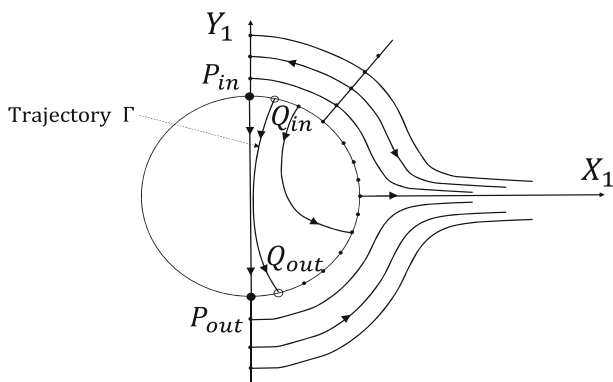


Fig. 7 Blow-up at the point S_C for system (1). Note that there is a trajectory connecting P_{in} to P_{out} on the hemisphere $\varepsilon_1 > 0$. This trajectory is in the plane $\{(X_1, Y_1, \varepsilon_1) | X_1 = 0, Y_1 = 0\}$ and corresponds to the vertical axis of the initial model (1) for $\varepsilon_1 > 0$. Moreover, we represent on this graph a trajectory Γ connecting Q_{in} to Q_{out} (open circles), which corresponds to a solution which may represent the trace of the limit cycle of system (1) on the hemisphere

to the dynamics of system (21), we focus here to the locus $\{X_1 \geq 0\}$. The vertical half straight line above the disk is the stable branch of the invariant manifold \Downarrow_{10} , the vertical half straight line below the disk is the unstable branch of this invariant manifold. The trajectory between the point P_{in} and the point P_{out} connects these branches on the hemisphere, explaining the occurrence of the canard solution. This solution is related to a delayed bifurcation (Vidal and Francoise 2012 or Rinaldi and Muratori 1992 for instance).

References

- Ambrosio B, Aziz-Alaoui MA, Yafia R (2018) Canard phenomenon in a slow–fast modified Leslie–Gower model. *Math Biosci* 295:48–54
- Auger P, Kooi BW, Bravo de la Parra R, Poggiale J-C (2006) Bifurcation analysis of a predator–prey model with predators using hawk and dove tactics. *J Theor Biol* 238:597–607
- Auger P, Bravo de la Parra R, Poggiale J-C, Sanchez E, Sanz L (2008) Aggregation methods in dynamical systems and applications in population and community dynamics. *Phys Life Rev* 5:79–105
- Benoit E, Callot JL, Diener F, Diener M (1981) Chasse au canard. *Coll Math* 32:37–119
- Boudjellaba H, Sari T (2009) Dynamical transcritical bifurcations in a class of predator–prey models. *J Differ Equ* 246:2205–2225
- Brøns M, Kaasen R (2010) Canards and mixed-mode oscillations in a forest pest model. *Theor Popul Biol* 77:238–242
- Cordoleani F, Nérini D, Morozov A, Gauduchon M, Poggiale J-C (2013) Scaling up the predator functional response in heterogeneous environment: when Holling type III can emerge? *J Theor Biol* 336:200–208
- de Feo O, Rinaldi S (1998) Singular homoclinic bifurcations in tritrophic food chains. *Math Biosci* 148:7–20
- Deng B (2001) Food chain chaos due to junction-fold point. *Chaos* 11(3):514–525
- Deng B, Hines G (2002) Food chain chaos due to Shilnikov's orbit. *Chaos* 12(3):533–538
- Dumortier F, Roussarie R (1996) Canard cycles and Center Manifolds, *Memoirs of the American Mathematical Society*, vol 121, issue 577
- Dumortier F, Roussarie R (2000) Geometric singular perturbation theory beyond normal hyperbolicity. In: Jones CKRT, Khibnik AI (eds) *Multiple time scale dynamical systems*. Springer, IMA p 122

- Fenichel N (1971) Persistence and smoothness of invariant manifolds for flows. *Indiana Univ Math J* 21:193–226
- Fenichel N (1979) Geometric singular perturbation theory for ordinary differential equation. *J Differ Equ* 31:53–98
- Flach EH, Schnell S (2006) Use and abuse of the Quasi-Steady-State Approximation. *IEE Proc Syst Biol* 153:187–191
- Françoise J-P, Piquet C, Vidal A (2008) Enhanced delay bifurcation. *Bull Belg Math Soc Simon Stevin* 15:825–831
- Hastings A (2016) Timescales and the management of ecological systems. *PNAS* 113:14568–14573
- Hek G (2010) Geometric singular perturbation theory in biological practice. *J Math Biol* 60:347–386
- Hirsch MW, Pugh CC, Shub M (1977) Invariant manifolds, lectures notes in mathematics, vol 583. Springer, Berlin
- Hoppensteadt F (1966) Stability in systems with parameter. *Trans Am Math Soc* 123:521–535
- Hsu SB (1978) On global stability of a predator–prey system. *Math Biosci* 39:1–10
- Hu H, Shen J, Zhou Z, Ou Z (2017) Relaxation oscillations in singularly perturbed generalized Liénard systems with non-generic turning points. *Math Model Anal* 22:389–407
- Jones CKRT (1994) Geometric singular perturbation theory. In: Johnson R (ed) *Dynamical systems, Montecatini Terme, lecture notes in mathematics*, vol 1609. Springer, Berlin, pp 44–118
- Kooi BW, Poggiale JC (2018) Modelling, singular perturbation and bifurcation analyses of bitrophic food chains. *Math Biosci* 301:93–110
- Kooi BW, Poggiale JC, Auger P, Kooijman SALM (2002) Aggregation methods in food chains with nutrient recycling. *Ecol Model* 157:69–86
- Krupa M, Szmolyan P (2001a) Relaxation oscillation and canard explosion. *J Differ Equ* 174:312–368
- Krupa M, Szmolyan P (2001b) Extending geometric singular perturbation theory to nonhyperbolic points-fold and canard points in two dimensions. *SIAM J Math Anal* 33:286–314
- Krupa M, Szmolyan P (2001c) Extending slow manifolds near transcritical and pitchfork singularities. *Nonlinearity* 4:1473–1491
- Kuehn C (2015) Multiple time scale dynamics, applied mathematical sciences, vol 191. Springer, Berlin
- Levin S (1985) Scale and predictability in ecological modeling in modeling and management of resources under uncertainty. In: Vincent TL, Cohen Y, Grantham WJ, Kirkwood GP, Skowronski JM (eds) *Lecture Notes in Biomathematics*, vol 72, pp 2–10
- Li C, Zhu H (2013) Canard cycles for predator–prey systems with Holling types of functional response. *J Differ Equ* 254:879–910
- Mehidi N (2001) A prey–predator–superpredator system. *J Biol Syst* 9(3):187–199
- Mehidi N, Sari T (1992) Limit cycles of a food chain system. In: *Proceedings of Pau congress*
- Muratori S, Rinaldi S (1992) Low- and high-frequency oscillations in three-dimensional Pau food chain systems. *SIAM J Appl Math* 52(6):1688–1706
- Poggiale JC (1998) Predator–prey models in heterogeneous environment: emergence of functional response. *Math Comput Model* 27:63–71
- Poggiale J-C, Auger P (1996) Fast oscillating migrations in a predator–prey model. *Math Mod Methods Appl Sci* 6:217–226
- Poggiale J-C, Auger P (2004) Impact of spatial heterogeneity on a predator–prey system dynamics. *CR Biol* 327:1058–1063
- Poggiale J-C, Gauduchon M, Auger P (2008) Enrichment paradox induced by spatial heterogeneity in a phytoplankton–zooplankton system. *Math Model Nat Phenom* 3:87–102
- Poggiale J-C, Auger P, Cordolani F, Nguyen-Huu T (2009) Study of a virus–bacteria interaction model in a chemostat: application of geometrical singular perturbation theory. *Philos Trans R Soc A* 367:4685–4697
- Pokrovskii A, Shchepakina E, Sobolev V (2008) Canard Doublet in a Lotka–Volterra type model. *J Phys Conf Ser* 138 <https://doi.org/10.1088/1742-6596/138/1/012019>
- Rinaldi S, Muratori S (1992) Slow–fast limit cycles in predator–prey models. *Ecol Model* 61:287–308
- Rosenzweig ML (1971) Paradox of enrichment: destabilization of exploitation ecosystems in ecological time. *Science* 171:385–387
- Sadhu S (2016) Canards and mixed-mode oscillations in a singularly perturbed two predators–one prey model. *Proc Dyn Syst Appl* 7:211–219
- Sakamoto K (1992) Invariant manifolds in singular perturbation problems for ordinary differential equations. *Proc R Soc Edinb* 116A:45–78

- Schauer M, Heinrich R (1983) Quasi-steady-state approximation in the mathematical modeling of biochemical reaction networks. *Math Biosci* 65:155–170
- Shoffner SK, Schnell S (2017) Approaches for the estimation of timescales in nonlinear dynamical systems: timescale separation in enzyme kinetics as a case study. *Math Biosci* 287:122–129
- Tikhonov AN (1952) Systems of differential equations containing small parameters in the derivatives. *Mat Sb* 31:575–586
- Vidal A, Francoise J-P (2012) Canard cycles in global dynamics. *Int J Bifurc Chaos* 22:1250026
- Vidyasagar M (1980) Decomposition techniques for large-scale systems with nonadditive interactions: stability and stabilizability. *IEEE Trans Autom Control* 25:773–779
- Wiggins S (1994) Normally hyperbolic invariant manifolds in dynamical systems, *App. Math. Sc. Series*. Springer, Berlin, p 105

Publisher's Note Springer Nature remains neutral with regard to jurisdictional claims in published maps and institutional affiliations.